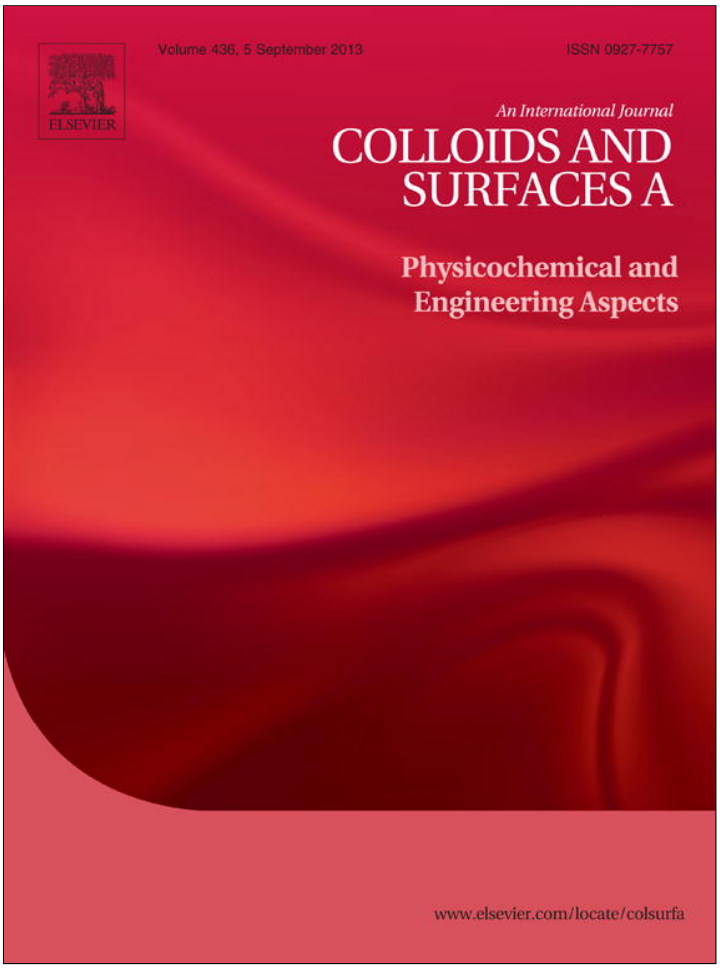

Colloids and Surfaces A: Physicochem. Eng. Aspects 436 (2013) 1000–1006

Contents lists available at ScienceDirect

Colloids and Surfaces A: Physicochemical and Engineering Aspects

journal homepage: www.elsevier.com/locate/colsurfa

Scaling laws in steady-state aqueous foams including Ostwald ripening

Joseph A. Attia, Sunny Kholi, Laurent Pilon*

Mechanical and Aerospace Engineering Department, University of California, Los Angeles, Los Angeles, CA 90095, USA

HIGHLIGHTS

- Equation governing the time rate of change of bubble radius in foams was scaled.
- A new dimensionless number accounting for Ostwald ripening was identified.
- It represents the ratio of the bubble contact time to gas permeation time.
- A new correlation was developed using experimental data for aqueous foams.
- Scaling law account for gravity, surface tension, and viscous forces and for gas diffusion.

GRAPHICAL ABSTRACT

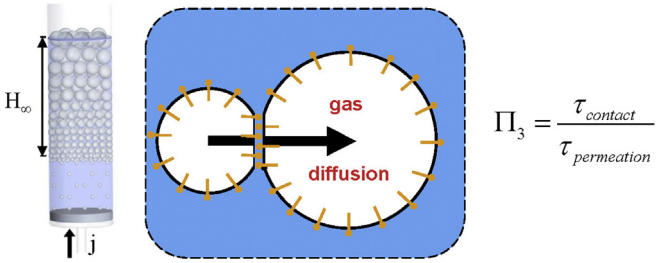

ARTICLE INFO

Article history:
Received 28 June 2013
Received in revised form 30 July 2013
Accepted 7 August 2013
Available online 17 August 2013

Keywords:
Pneumatic foams
Bubble columns
Dimensional analysis
Disproportionation
Interbubble gas diffusion
Multiphase flow

ABSTRACT

This paper presents scaling laws governing the steady-state behavior of pneumatic foams produced by injecting gas in aqueous surfactant solutions under isothermal conditions. Dimensional analysis of the governing equation for the time rate of change of bubble radius in foams due to Ostwald ripening yielded a dimensionless similarity parameter representing the ratio of the average contact time between bubbles to the characteristic time for gas permeation. This dimensionless number was combined with two other dimensionless numbers previously derived for high viscosity fluids and ignoring foam coarsening. Semi-empirical parameters of a power-law relation between these three dimensionless numbers were determined from experimental data collected in the present study as well as from the literature for various gases and aqueous surfactant solutions. They cover a wide range of physical parameters including foam thickness, superficial gas velocity, solubility, surface tension, and average bubble radius.

1. Introduction

Liquid foams are an important component of numerous technologies including petrochemical [1], pharmaceutical [2], food [3,4], and water treatment processes [5], as well as glass [6], iron, and steel manufacturing [7–9]. Depending on the application, foams may prove either beneficial or detrimental. In water treatment, for example, foam is generated by injecting gas bubbles into wastewater and collected to separate organic waste (i.e., proteins) or impurities from water streams [5]. In such separation processes, foaming agents are typically utilized to achieve faster separation and easier waste disposal [5]. Given the range of applications, a better understanding of foam formation and stability is essential for predicting and controlling foam behavior in these various processes.

Bubble coalescence and Ostwald ripening can significantly affect the behavior of foams made from low viscosity fluids [10]. The combination of these two phenomena has been termed "foam coarsening." On the one hand, bubble coalescence occurs when two adjacent bubbles merge as a result of rupture of the films separating

* Corresponding author. Tel.: +1 310 206 5598; fax: +1 310 206 4830.
E-mail address: pilon@seas.ucla.edu (L. Pilon).

0927-7757/$ – see front matter © 2013 Elsevier B.V. All rights reserved.
http://dx.doi.org/10.1016/j.colsurfa.2013.08.025

Nomenclature

A	surface area of bubble in foam (m^2)
D	diffusion coefficient (m^2/s)
$f_1(r, t)$	bubble size distribution in the foam (m)
g	specific gravity (m/s^2)
$H(t)$	transient foam thickness (m)
H_∞	steady-state foam thickness (m)
J	effective gas permeability [Eq. (11)]
j	superficial gas velocity (m/s)
j_m	superficial gas velocity for onset of foaming (m/s)
k	effective gas permeability [Eq. (9)]
k_{ml}	monolayer gas permeability or bubble lamella permeability (m/s)
K, L, m, n	semi-empirical constants
N	number of moles of gas inside a bubble (mol)
p_g	pressure in the gas bubble (Pa)
p_l	pressure in the liquid phase (Pa)
R	universal gas constant (=8.314 J/mol K)
r	bubble radius in the foam (m)
r_m	mean bubble radius in the foam (m)
r_0	average bubble radius at the bottom of the foam (m)
S_O	Ostwald solubility coefficient
T	temperature (K)
t	time (s)

Greek symbols

δ_f	thickness of the fluid region bounded by Plateau borders (m)
μ	dynamic viscosity of the liquid phase (Pa· s)
Π_i	dimensionless similarity parameters, i = 1, 2, 3
ρ	density (kg/m^3)
σ	surface tension (N/m)
τ_c, τ_d	characteristic times of contact and permeation between bubbles (s)

Superscript

*	refers to dimensionless properties

them [11]. This process simultaneously increases the mean bubble size while decreasing the number of bubbles and the liquid–gas interfacial area. On the other hand, Ostwald ripening, also called interbubble gas diffusion or disproportionation, describes mass transfer from small bubbles with higher internal pressure to large bubbles at lower pressure [12]. It causes larger bubbles to grow at the expense of smaller ones. These larger bubbles are less stable and separated by thinner liquid films, making them more prone to coalesce [10,13,14]. They, then, burst and discharge the liquid contained in the film which drains through the foam. Ostwald ripening is enhanced when the solubility and the diffusion coefficient of the gas in the liquid phase are large [12,14,15].

At early times in the foam's life, bubbles accumulate at the liquid surface surrounded by relatively thick liquid films. The foam grows at its largest rate as no bubble burst at the top. In this phase, mass balance of the gas phase in the foams leads to the following expression for the transient foam thickness $H(t)$ [16]

$$H(t) = \frac{j}{\overline{\phi}}t \quad \text{with} \quad \overline{\phi}(t) = \frac{1}{H(t)}\int_0^{H(t)} \phi(z,t)\mathrm{d}z \tag{1}$$

where j is the superficial gas velocity (in m/s) and $\overline{\phi}$ is the average foam porosity while $\phi(z, t)$ is the local foam porosity at height z and time t [16]. The latter was suggested to be taken as 0.82 for all practical purposes [16]. As the foam ages and liquid drainage takes place, adjacent bubbles are more prone to coalesce when the film separating them is thin and more likely to rupture. This phenomenon dominates at the top of the foam column where the bubbles are the oldest and the foam is dry [17]. Soon after the first bubbles burst at the top of the foam which reaches a steady-state height H_∞ when the incoming flow of gas at the bottom of the foam matches the amount of gas released by bubbles bursting at the top.

Moreover, Pilon et al. [18] investigated the behavior of liquid foams formed by injecting gas bubbles into viscous fluids under steady-state and isothermal conditions. The authors performed a scaling analysis of the governing equation for the time-dependent foam thickness [17]. The model accounted for the effects of viscous, gravitational, and capillary forces. However, it neglected both bubble coalescence and interbubble gas diffusion because the viscosity of the fluid was large and the films separating the bubbles was consequently thick and relatively stable. Two dimensionless numbers were identified as describing the steady-state behavior of liquid foams generated from high viscosity liquids [18],

$$\Pi_1 = \frac{\rho g r_0^2}{\mu(j - j_m)} \quad \text{and} \quad \Pi_2 = \frac{\mu H_\infty (j - j_m)}{\sigma r_0} \tag{2}$$

where ρ and μ are the fluid density and dynamic viscosity, respectively. The average bubble radius at the bottom of the foam and the steady-state foam thickness are denoted by r_0 and H_∞, respectively, while j is the superficial gas velocity and j_m is the minimum superficial gas velocity for onset of foaming [19]. The dimensionless parameter Π_1 can be interpreted as the ratio of the gravitational force to the viscous force on an average bubble of radius r_0 having a velocity $(j - j_m)$. Similarly, Π_2 corresponds to the ratio of the viscous force to the surface tension force multiplied by the ratio H_∞/r_0 scaling the steady-state foam height by the average bubble radius. The relationship between Π_1 and Π_2 was assumed to follow the power-law relation $\Pi_2 = K\Pi_1^n$ where empirical coefficients K and n were found to be 2905 and −1.8, respectively, from more than 120 experimental data points for foams formed from high viscosity liquids such as water containing glycerine, molten slag, and glass [18]. Bubbles were formed by injecting nitrogen, air, or argon through single, multi-orifice nozzles, or a porous medium. The experimental data featured a wide range of physicochemical properties, types of gas, bubble radius, and gas flow rates. Comparison between the developed semi-empirical correlation and the experimental data yielded reasonable agreements given the broad bubble size distribution around the mean value as well as uncertainties in H_∞, and in the thermophysical properties. For low viscosity fluids (e.g., aqueous surfactant solutions), however, the above correlation was shown to be inappropriate [20,21]. Interestingly, the parameter K changed with the type of gas while n was almost the same and equal to −1.8 for all gases. Deviations from the correlation developed for highly viscous fluids was attributed to foam coarsening that becomes significant for low viscosity fluids but was neglected in the formulation of the governing equations leading to the definition of the dimensionless numbers Π_1 and Π_2.

The present study aims to demonstrate the existence of a third dimensionless similarity parameter governing steady-state aqueous foams accounting for Ostwald ripening. It will enable one to predict the steady-state thickness of aqueous foams from thermophysical properties of the liquid and gas phases and the operating conditions.

2. Experiments

Fig. 1 depicts the experimental setup used in this study. Foam was generated by continuously injecting air through a fritted disc into a vertical glass column (Wilmad-Lab Glass) of diameter 50.8 mm and height 30.0 cm. The fritted disc located at the

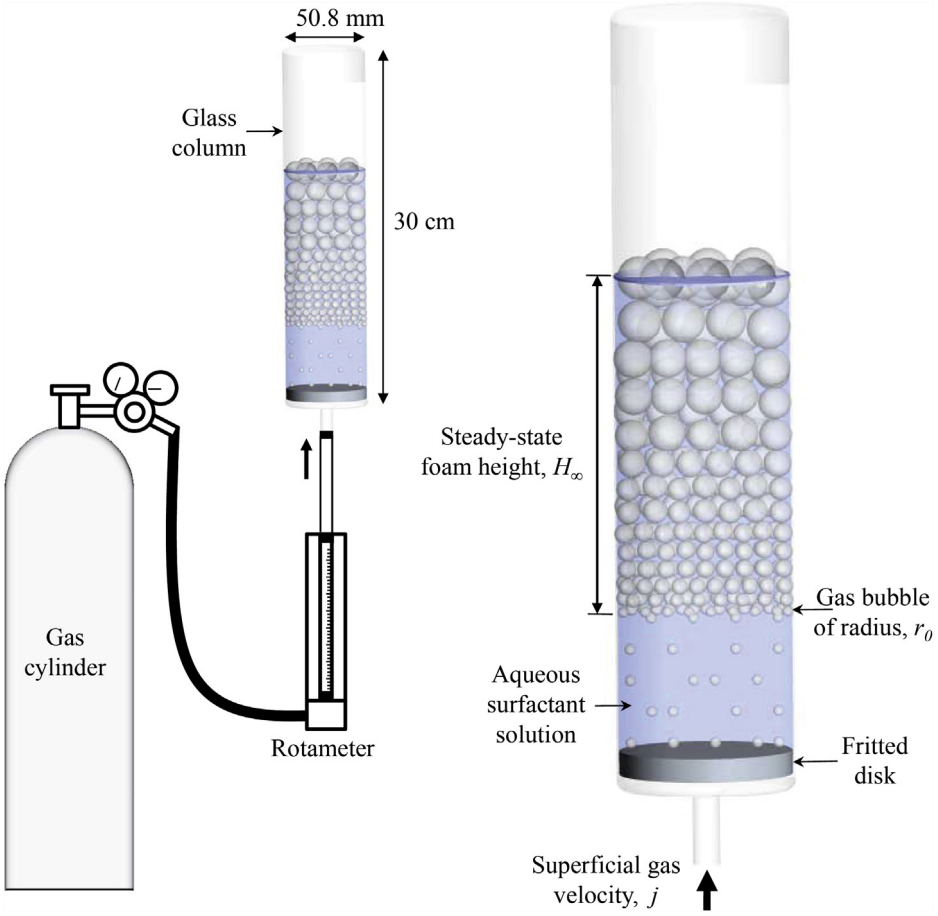

Fig. 1. Schematic of the experimental setup used in this study to investigate aqueous pneumatic foams.

bottom of the glass column was 4 mm thick, had coarse porosity (10–15 μm), and spanned the entire column cross-section. The aqueous surfactant solution was made by mixing sodium dodecyl sulfate (SDS) surfactant (99%, Fisher Scientific) in deionized water to achieve SDS mass fraction of 0.4 wt.% or 19.9 mg/l of water. The column and the fritted disc were thoroughly washed and the inner walls of the column were wetted before each measurement to ensure uniform wall conditions and to remove any impurity that could obstruct the growth of the foam in the column. The column was filled with 136 ml of aqueous surfactant solution and dry air was bubbled through for several minutes to saturate the solution before starting the measurements. All measurements were performed at room temperature. The air flow rate was measured using an Omega FT-042-15-G1-VN rotameter. The foam height $H(t)$ was visually measured as a function of time using a laboratory grade scale mounted along the glass column. Photographs of the gas bubbles at the bottom of the foam were taken with a Nikon D90 DSLR camera with a Nikon 55-200 mm VR lens. Image processing software (ImageJ) was used to determine the bubble size distribution at the bottom of the foam column. The associated experimental uncertainties were estimated to be (i) ±13 mm for foam height $H(t)$ and H_∞ measurements and (ii) ±0.1 mm for the bubble radii. Measurements of the foam thickness and bubble radius were repeated at least three times for each value of superficial gas velocity considered.

3. Analysis

Liquid drainage, bubble coalescence, and Ostwald ripening must take their course before the foam reaches a steady state. Experimentally it takes typically dozens of minutes to several hours to achieve steady-state conditions when generating foam in a bubble column [20,22]. This time scale is on the same order of magnitude as the characteristic time for Ostwald ripening [12]. On the other hand, the characteristic time for coalescence is on the order of 1–10 min [12]. Experimental observations have also demonstrated that the type of gas had significant effect on the steady-state thickness of foams made from aqueous surfactant solutions [21]. These observations indicate that Ostwald ripening is an essential phenomenon controlling the steady-state foam thickness. The following assumptions were made in developing a physical model and the associated scaling analysis accounting for Ostwald ripening (1) isothermal conditions were maintained in the foam, (2) thermophysical properties of the gas and liquid phases remained constant within the foam, (3) the bubbles within the foam were treated as spherical.

3.1. Governing equation

The pressure difference between the gas inside a bubble of radius r and the liquid within the foam can be expressed as [13],

$$p_g - p_l = 2\sigma\left(\frac{1}{r_m} - \frac{1}{r}\right), \tag{3}$$

where p_g and p_l are the pressures in the gas and liquid phases, respectively. Here, r is the radius of the bubble of interest and r_m is the mean bubble radius defined as [13],

$$r_m(t) = \frac{\int_0^\infty r^2 f_1(r,t)\mathrm{d}r}{\int_0^\infty r f_1(r,t)\mathrm{d}r}, \tag{4}$$

where $f_1(r,t)$ is the bubble size distribution within the foam at time t. Bubble growth or shrinkage is determined from the difference between r and r_m, i.e., if $r > r_m$ the bubble grows while if $r < r_m$ the bubble shrinks.

Moreover, the molar mass transfer rate from a bubble of radius r to the liquid phase can be expressed as [13],

$$\frac{dN}{dt} = \frac{kA}{RT}(p_g - p_l), \tag{5}$$

where N represents the number of moles of gas within a bubble of radius r, while k is the effective gas permeability expressed in m/s. The surface area of the bubble is $A = 4\pi r^2$, while R = 8.314 J/mol K is the universal gas constant and T is the absolute temperature. Combining Eqs. (3) and (5) yields,

$$\frac{dN}{dt} = \frac{8\pi k\sigma}{RT}\left(\frac{r^2}{r_m} - r\right). \tag{6}$$

Assuming that the gas inside the bubbles behaves as an ideal gas, the number of moles within a spherical bubble can be expressed as,

$$N = \frac{4\pi r^3 p_g}{3RT}. \tag{7}$$

Assuming that p_g is constant and slightly above atmospheric pressure, as suggested by Lemlich [13], and combining Eqs. (6) and (7) yields,

$$\frac{dr}{dt} = \frac{2k\sigma}{p_g}\left(\frac{1}{r_m} - \frac{1}{r}\right). \tag{8}$$

The effective gas permeability k from bubbles across liquid films was defined by Princen and Mason [23] and expressed in terms of the thermophysical properties of the gas and liquid phases as,

$$k = \frac{DS_O}{\delta_f + 2D/k_{ml}}, \tag{9}$$

where k_{ml} is the permeability of a monolayer of surfactants surrounding the bubble and δ_f is the thickness of the liquid film separating two adjacent bubbles. The diffusion coefficient of the gas in the liquid phase is denoted by D and is assumed to be constant. The Ostwald coefficient of solubility is denoted by S_O (dimensionless) and is defined as the volume of saturated gas absorbed by unit volume of pure liquid at given temperature and pressure [24].

Princen and Mason [23] simplified Eq. (9) for two limiting cases: (i) when gas permeation is controlled by the surfactant monolayer, i.e. $\delta_f \ll 2D/k_{ml}$ and (ii) when gas permeation is controlled by the liquid layer or $\delta_f \gg 2D/k_{ml}$. In the first case, the diffusivity or effect of interbubble gas diffusion is negligible. This is contrary to the pronounced effects of the gas type on the foam behavior observed in low viscosity fluid foams [13,21]. Instead, one can assume that gas permeation is controlled by the liquid layer, i.e., $\delta_f \gg 2D/k_{ml}$. The effective gas permeability k, therefore, simplifies to $k = DS_O/\delta_f$. Then, the time rate of change in bubble radius is expressed as,

$$\frac{dr}{dt} = \frac{2DS_O\sigma}{p_g\delta_f}\left(\frac{1}{r_m} - \frac{1}{r}\right). \tag{10}$$

Note that Eq. (10) is similar to the expression for the time rate of change in bubble radius due to interbubble gas diffusion proposed by Lemlich [13] as,

$$\frac{dr}{dt} = \frac{2J\sigma RT}{p_g}\left(\frac{1}{r_m} - \frac{1}{r}\right), \tag{11}$$

where J is the effective gas permeability and was defined in terms of the volumetric fraction of liquid in the foam, the second and third moments of the bubble size distribution, the diffusion coefficient, and Henry's law constant [13].

3.2. Dimensional analysis

In order to scale Eq. (10), the following independent dimensionless variables were introduced

$$r^* = \frac{r}{r_0}, \quad \sigma^* = \frac{\sigma}{p_0 r_0}, \quad \delta_f^* = \frac{\delta_f}{r_0}, \quad p_g^* = \frac{p_g}{p_0},$$
$$\text{and} \quad t^* = \frac{t}{\tau_c} = \frac{t}{r_0/(j - j_m)} \tag{12}$$

where r_0 is the average bubble radius at the bottom of the foam layer [18] taken as the characteristic length, $\tau_c = r_0/(j - j_m)$ is the characteristic contact time between a rising bubble and a bubble at rest in the foam, and p_0 is the atmospheric pressure. Substituting Eq. (12) into Eq. (10) yields the following dimensionless governing equation,

$$\frac{dr^*}{dt^*} = \frac{2DS_O}{r_0(j - j_m)}\left[\frac{\sigma^*}{p_g^*\delta_f^*}\left(\frac{1}{r_m^*} - \frac{1}{r^*}\right)\right]. \tag{13}$$

Then, a third dimensionless number Π_3 accounting for interbubble gas diffusion can be identified as,

$$\Pi_3 = \frac{DS_O}{r_0(j - j_m)} = \frac{\tau_c}{\tau_d} \tag{14}$$

This dimensionless number can be interpreted as the ratio of the average contact time between bubbles in the foam $\tau_c = r_0/(j - j_m)$ and the characteristic permeation time defined as $\tau_d = {r_0}^2/(DS_O)$. It could also be expressed as $\Pi_3 = S_O/Pe_{r_0}$ where Pe_{r_0} is the Péclet number for mass transfer defined as the the ratio of advection and diffusion mass transfer rates.

The Buckingham–Pi theorem provides an alternative way of identifying Π_3. This approach is analogous to the treatment undertaken by Lotun and Pilon [25] in modeling slag foaming where the steady-state thickness H_∞ was assumed to depend on six variables namely $\rho, g, \mu, \sigma, (j - j_m)$, and r_0. Their analysis led to four dimensionless numbers which can be combined to yield Π_1 and Π_2 given by Eq. (2). Here, two additional variables, D and S_O, were introduced to account for Ostwald ripening. Two dimensionless groups were identified, in addition to the four dimensionless numbers derived by Lotun and Pilon [25]. The first new dimensionless group was identified as $\Pi_5 = S_O$ and the second was $\Pi_6 = \frac{D}{r_0(j - j_m)}$. Multiplying these two new dimensionless groups yields Π_3 given by Eq. (14). Thus, both approaches give consistent dimensionless numbers. Finally, the relationship between Π_1, Π_2, and Π_3 is assumed to follow a power-law relation given by

$$\Pi_2 = L\Pi_1^n\Pi_3^m, \tag{15}$$

where L, n, and m are semi-empirical constants determined from experimental data.

4. Results and discussion

4.1. Experimental results

Fig. 2 plots the temporal evolution of the average foam height for superficial gas velocity j equal to 0.015 and 0.018 mm/s. Each data point represents the average of at least three independent runs for each value of j. The error bars correspond to 95% confidence interval and indicate that measurements were reproducible from the transient foam growth to its steady state. Fig. 2 also plots the transient foam height predicted by Eq. (1) using $\bar{\phi}$ = 0.82. Good agreement between experimental data and model predictions was observed early in the foaming process. As previously mentioned, Eq. (1) is based on the assumption that gas accumulates but does not escape the control volume defined by the foam. Despite interbubble gas

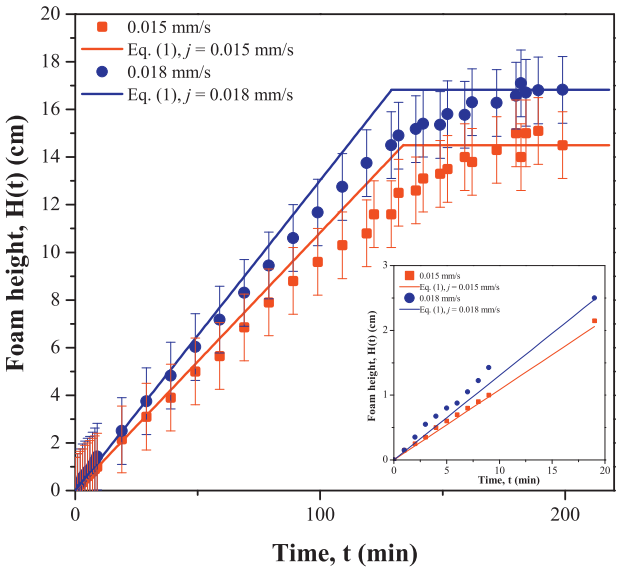

Fig. 2. Evolution of foam height as a function of time and superficial gas velocity. Solid and dashed lines represent transient foam height model [16] as a function of superficial gas velocity.

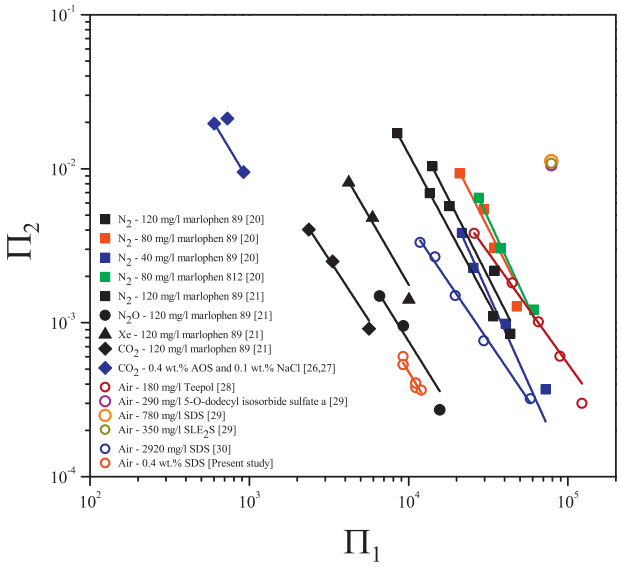

Fig. 3. Relationship between Π_2 vs. Π_1 for aqueous foams made from different surfactant solutions and gases measured in the present study and reported in the literature [20,21,26–30]. Experimental conditions and fluid properties are summarized in Table 1.

diffusion, the gas remains within the foam. Thus, Ostwald ripening does not affect the early foam growth rate. However, it affects the time at which bubbles start bursting at the top of the foam. In fact, experimental data deviated from the model predictions as the foam approached its steady-state height H_∞. Moreover, the average residence time of a bubble in the foam can be estimated as H_∞/j which was equal to more than 2 hours for j=0.015 and 0.018 mm/s. This time scale confirms that Ostwald ripening played an important role in the steady-state behavior of the aqueous foams investigated.

4.2. Scaling analysis

The steady-state foam thickness data collected in the present study along with those reported in the literature [20,21,26–30] for foams made by injecting oxygen, nitrous oxide, nitrogen, xenon, air, or carbon dioxide gases into various aqueous surfactant solutions were used to validate the previously described scaling analysis. Table 1 summarizes the experimental conditions and the liquid and gas properties corresponding to these various studies. The viscosity of water at room temperature was estimated from the DIPPR database. The surface tension of the 0.4 wt.% SDS aqueous solution was reported to be 40.8 mN/m [31]. The Ostwald coefficient of solubility S_O for each gas in water at 293 K was reported by Hartland et al. [21]. The gas diffusion coefficient in water D was also reported by Hartland et al. [21] and calculated from the correlation developed by Wilke and Chang [32] accounting for the viscosity, temperature, and molecular weight of the gases. Additionally, the diffusion coefficient of carbon dioxide in water was reported by Feitosa et al. [26]. The properties of air were approximated as those of nitrogen. Overall, the experimental data covered a wide range of physical parameters associated with the foam formation process, i.e., $0.02 \le j \le 0.78$ mm/s, $0.0 \le j_m \le 0.1$ mm/s, $0.1 \le r_0 \le 2.5$ mm, $1.26\times10^{-9} \le D \le 1.8\times10^{-9}$ m^2/s, $0.02 \le S_O \le 0.92$, and $31.1 \le \sigma \le 41.1$ mN/m corresponding to H_∞ varying between 26 and 1390 mm. Note that the experimental data considered focused exclusively on aqueous foams and do not present any significant fluctuations in viscosity ($\mu \approx 1.22$ mPa/s) and density ($\rho \approx 1014$ kg/m^3). A total of 51 different data points were collected resulting in dimensionless numbers Π_1 ranging from 602 to 122,625, Π_2 varying between 3×10^{-4} and 2.1×10^{-2}, and Π_3 from 1×10^{-5} to 6.2×10^{-2}.

Fig. 3 plots Π_2 versus Π_1 for foams made by injecting various gases in aqueous surfactant solutions [20,21,26–30]. Unlike what was observed for high viscosity fluids [18], experimental data for aqueous foams did not collapse on a single line. However, the different data sets shows similar trend expressed as $\Pi_2 = K(\Pi_3)\Pi_1^n$ where the semi-empirical function $K(\Pi_3)$ depends on Π_3, i.e., $K(\Pi_3) = L\Pi_3^m$. Our previous study [18] estimated n to be −1.8 not only for both high viscosity fluids but also for low viscosity fluids albeit for a subset of the experimental data considered in the present study [20,21]. Here, the datasets considered is much larger and broader and least squares fitting also yielded a value of n close to −1.8.

Moreover, Fig. 4 plots $\Pi_1^{1.8}\Pi_2$ versus Π_3 for the same data shown in Fig. 3. Eq. (15) appears to fit experimental data over a wide range of thermophysical properties with the parameters L = 118 and m = −0.96 with a coefficient of determination $R^2_{corr} = 0.95$. Fig. 4

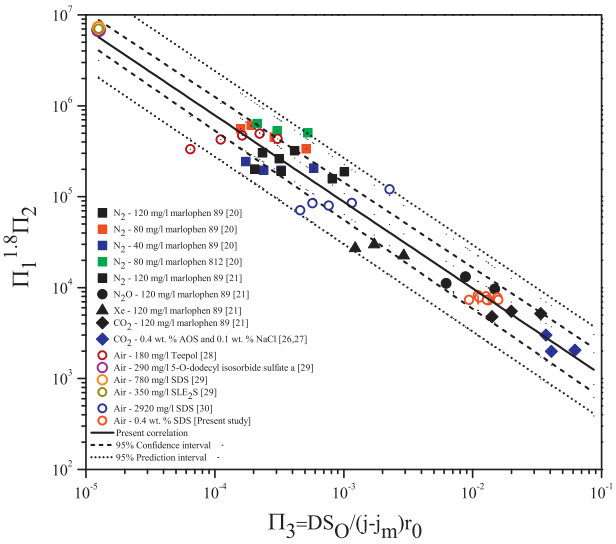

Fig. 4. Correlation between dimensionless numbers $\Pi_2\Pi_1^{1.8}$ and Π_3 for aqueous foams made from different surfactant solutions and gases as summarized in Table 1. The same data sets are presented in Fig. 3.

Table 1
Experimental conditions and thermophysical properties for different gases injected in aqueous surfactant solutions [20,21,26–30].

Aqueous solution of	Conc. (mg/l)	Gas	σ (mN/m)	μ (mPa s)	ρ (kg/m^3)	D (m^2/s)	S_O	Ref.
10% glycerine + marlophen 89	120	N_2	32.1	1.22	1014	1.45×10^{-9}	1.69×10^{-2}	
10% glycerine + marlophen 89	80	N_2	35.4	1.22	1014	1.45×10^{-9}	1.69×10^{-2}	
10% glycerine + marlophen 89	40	N_2	41.1	1.22	1014	1.45×10^{-9}	1.69×10^{-2}	[20]
10% glycerine + marlophen 812	80	N_2	36.3	1.22	1014	1.45×10^{-9}	1.69×10^{-2}	
10% glycerine + marlophen 89	120	N_2	32.1	1.22	1014	1.45×10^{-9}	1.7×10^{-2}	
10% glycerine + marlophen 89	120	NO_x	31	1.22	1014	1.43×10^{-9}	67.6×10^{-2}	
10% glycerine + marlophen 89	120	Xe	31.52	1.22	1014	1.26×10^{-9}	12.1×10^{-2}	[21]
10% glycerine + marlophen 89	120	CO_2	31.13	1.22	1014	1.43×10^{-9}	91.9×10^{-2}	
0.4 wt.% AOS and 0.01 wt.% NaCl	–	CO_2	44.0	1.10	1000	1.80×10^{-9}	91.9×10^{-2}	[26]
0.4 wt.% AOS and 0.01 wt.% NaCl	–	CO_2	44.0	1.10	1000	1.80×10^{-9}	91.9×10^{-2}	[27]
Teepol	4120	Air[a]	40.0	1.0	1000	1.45×10^{-9}	1.69×10^{-2}	[28]
SDS	7800	Air[a]	36.3	1.0	1000	1.45×10^{-9}	1.69×10^{-2}	
5-O-dodecyl isosorbide sulfate a	2900	Air[a]	41.2	1.0	1000	1.45×10^{-9}	1.69×10^{-2}	[29]
SLE_2S	3500	Air[a]	39.6	1.0	1000	1.45×10^{-9}	1.69×10^{-2}	
SDS	2920	Air[a]	40.0	1.0	1000	1.45×10^{-9}	1.69×10^{-2}	[30]
0.4 wt.% sodium dodecyl sulfate (SDS)	19.9	Air[a]	40.8	0.9	1000	1.45×10^{-9}	1.69×10^{-2}	This study

[a] Properties of N_2 assumed in analysis.

also shows the 95% confidence and prediction intervals for the derived power-law relationship. Note that the derived correlation spans four and five orders of magnitude in terms of $\Pi_1^{1.8}\Pi_2$ and Π_3, respectively. Furthermore, the average relative error between model predictions given by Eq. (15) and the 95% confidence and prediction intervals was less than ±4% and ±10%, respectively. Such spread is expected in two-phase flow, particularly for foams given (1) their inherent metastability, (2) the different interdependent physical phenomena (i.e., drainage, Ostwald ripening, and bubble coalescence) and (3) the resulting experimental uncertainty. Differences between experimental data and power law predictions can be attributed to two primary factors: (i) the limited amount of data available for steady-state thicknesses of foams generated with low viscosity solutions and (ii) the uncertainties of the actual measured physical quantities (i.e., r_0, H_∞, D) used to estimate the dimensionless number Π_1, Π_2, and Π_3. For instance, typical uncertainties include ±5% for the variation in measured foam thickness [20], and ±10% for the diffusion coefficient estimated by the model presented by Wilke and Chang [32]. Additionally, measurements of bubble radius, particularly, in cases where the radius is visually determined, have been shown to be a significant source of experimental uncertainty [33]. Furthermore, due to increased interbubble gas diffusion in lower viscosity fluids, the use of the average radius r_0 in the dimensional analysis is clearly a first order approximation as bubbles change size as they rise through the foam. Lastly, as pointed out in previous studies [18], differences between correlation predictions and experimental data were larger in cases when the superficial gas velocity approached j_m corresponding to smaller foam thicknesses.

In order to identify the significant physical phenomena influencing the steady-state foam thickness, Eq. (15) can be expressed in dimensional form as,

$$H_\infty = 118 \frac{\sigma}{r_0^{1.64}} \frac{\mu^{0.8}(j - j_m)^{1.76}}{(\rho g)^{1.8}(DS_O)^{0.96}}. \quad (16)$$

The effects of gravity, liquid viscosity, and density captured by Π_1 and Π_2 have been discussed previously and need not be reported [18]. Only the effects of parameters appearing in Π_3 should be discussed. Eq. (16) indicates that the steady-state foam thickness decreases as either the Ostwald solubility coefficient S_O or the diffusion coefficient D increases. As previously discussed, coarsening destabilizes the foam and is enhanced by larger values of D and S_O. In addition, the steady-state foam thickness increases with increasing superficial gas velocity j. This is consistent with experimental observations [18,20,21]. Foam thickness has also been shown to be significantly dependent on bubble radius r_0 [20] as evidenced by the associated exponent of 1.7 in Eq. (16). Moreover, Ogawa *et al.*[34] experimentally established that the bubble radius is linearly proportional to surface tension σ. Therefore, Eq. (16) suggests that increasing σ causes the ratio $\sigma/r_0^{1.76}$, and therefore H_∞, to decrease.

5. Conclusions

This paper presented a dimensional analysis of the governing equation for the time rate of change of bubble radius in foams accounting for Ostwald ripening. It led to the definition of a dimensionless number accounting for the effects of both the diffusion and solubility of the particular gas in the liquid phase identified as $\Pi_3 = DS_O/(j - j_m)r_0$. It represents the ratio of the average contact time between bubbles to the characteristic time for gas permeation. This number was combined with the dimensionless numbers Π_1 and Π_2 identified by Pilon et al. [18] and accounting for viscous, surface tension, and gravitational forces. Note that the same dimensionless number was also obtained by applying the Buckingham–Pi theorem to the relevant variables associated with steady-state foam thickness. A new power-law relation between Π_1, Π_2, and Π_3 was determined as $\Pi_2 = 118\Pi_1^{-1.8}\Pi_3^{-0.96}$ based on experimental data reported in the literature [20,21,26–30]. These results can be used in a wide range of applications such as petrochemical, pharmaceutical, food, and water treatment processes.

References

[1] L.L. Schramm, E.E. Isaacs, Foams in enhancing petroleum recovery, in: P. Stevenson (Ed.), Foam Engineering: Fundamentals and Applications, Wiley-Blackwell, United Kingdom, 2012, pp. 149–160.
[2] C.E. Lockwood, P.M. Bummer, M. Jay, Purification of proteins using foam fractionation, Pharm. Res. 14 (11) (1997) 1511–1515.
[3] G. Narsimhan, A model for unsteady state drainage of a static foam, J. Food Eng. 14 (1991) 139–165.
[4] R.J. Germick, A.S. Rehill, G. Narsimhan, Experimental investigation of static drainage of protein stabilized foams – comparison with model, J. Food Eng. 23 (1994) 555–578.
[5] I.A. Eldib, Foam fractionation for removal of soluble organics from wastewater, Res. J. Water Pollut. Control Fed. 33 (9) (1961) 914–931.
[6] L. Pilon, Foams in glass manufacturing, in: P. Stevenson (Ed.), Foam Engineering, John Wiley & Sons Ltd., UK, 2012, pp. 149–160.

[7] K. Ito, R.J. Fruehan, Study of the foaming of CaO-SiO_2-FeO slags: part II. Dimensional analysis and foaming in iron and steelmaking processes, Metall. Mater. Trans. B 20B (1989) 515–521.
[8] R. Jiang, R.J. Fruehan, Slag foaming in bath smelting, Metall. Mater. Trans. B 22B (1991) 481–489.
[9] S-M. Jung, R.J. Fruehan, Foaming characteristics of BOF slags, ISIJ Int. 40 (2000) 348–354.
[10] F.G. Gandolfo, H.L. Rosano, Interbubble gas diffusion and the stability of foams, J. Colloid Interface Sci. 194 (1997) 31–36.
[11] A. Colin, Coalescence in foams, in: P. Stevenson (Ed.), Foam Engineering, John Wiley & Sons Ltd., UK, 2012, pp. 75–90.
[12] O. Pitois, Foam ripening, in: P. Stevenson (Ed.), Foam Engineering, John Wiley & Sons Ltd., UK, 2012, pp. 59–73.
[13] R. Lemlich, Prediction of changes in bubble size distribution due to interbubble gas diffusion in foam, Ind. Eng. Chem. Fundam. 17 (2) (1978) 89–93.
[14] S. Hilgenfeldt, S. Koehle, H. Stone, Dynamics of coarsening foams: accelerated and self-limiting drainage, Phys. Rev. Lett. 86 (20) (2001) 4704–4707.
[15] S. Tcholakova, Z. Mitrinova, K. Golemanov, N.D. Denkov, M. Vethamuthu, K.P. Ananthapadmanabhan, Control of Ostwald ripening by using surfactants with high surface modulus, Langmuir 27 (2011) 14807–14819.
[16] L. Pilon, A.G. Fedorov, R. Viskanta, Analysis of transient thickness of pneumatic foams, Chem. Eng. Sci. 57 (2002) 977–990.
[17] A. Bhakta, E. Ruckenstein, Decay of standing foams: drainage, coalescence and collapse, Adv. Colloid Interface Sci. 70 (1997) 1–124.
[18] L. Pilon, A.G. Fedorov, R. Viskanta, Steady-state foam thickness of liquid–gas foams, J. Colloid Interface Sci. 242 (2001) 425–436.
[19] L. Pilon, R. Viskanta, Minimum superficial gas velocity for onset of foaming, Chem. Eng. Process. 43 (2) (2004) 149–160.
[20] S.A.K. Jeelani, S. Ramaswami, S. Hartland, Effect of binary coalescence on steady-state height of semi-batch foams, Trans. Inst. Chem. Eng. A 68 (1990) 271–277.
[21] S. Hartland, J.R. Bourne, S. Ramaswami, A study of disproportionation effects in semi-batch foams – II. Comparison between experiment and theory, Chem. Eng. Sci. 48 (1993) 1723–1733.
[22] S. Hartland, A.D. Barber, A model for cellular foam, Trans. Inst. Chem. Eng. 52 (1974) 43–52.
[23] H.M. Princen, S.G. Mason, The permeability of soap films to gases, J. Colloid Sci. 20 (1965) 353–375.
[24] R. Battino, The Ostwald coefficient of gas solubility, Fluid Phase Equilib. 15 (1984) 231–240.
[25] D. Lotun, L. Pilon, Physical modeling of slag foaming for various operation conditions and slag compositions, ISIJ Int. 45 (6) (2005) 835–840.
[26] K. Feitosa, O.L. Halt, R.D. Kamien, D.J. Durian, Bubble kinetics in a steady-state column of aqueous foam, Europhys. Lett. 76 (2006) 683–689.
[27] K. Feitosa, D.J. Durian, Gas and liquid transport in steady-state aqueous foam, Eur. Phys. J. E 26 (2008) 309–316.
[28] S.J. Neethling, H.T. Lee, P. Grassia, The growth, drainage and breakdown of foams, Colloid. Surf. A: Physicochem. Eng. Aspects 263 (2005) 184–196.
[29] A. Lavergne, Y. Zhu, A. Pizzino, V. Molinier, J.M. Aubry, Synthesis and foaming properties of new anionic surfactants based on a renewable building block: Sodium dodecyl isosorbide sulfates, J. Colloid Interface Sci. 360 (2) (2011) 645–653.
[30] X. Li, R. Shaw, P. Stevenson, Effect of humidity on dynamic foam stability, Int. J. Miner. Process. 94 (2010) 14–19.
[31] J. Zhao, S. Pillai, L. Pilon, Rheology of colloidal gas aphrons (microfoams) made from different surfactants, Colloid. Surf. A: Physicochem. Eng. Aspects 348 (2009) 93–99.
[32] R. Wilke, P. Chang, Correlation of diffusion coefficients in dilute solutions, Amer. Inst. Chem. Eng. J. 1 (1955) 264–270.
[33] H. Cheng, R. Lemlich, Errors in the measurement of bubble size distribution in foam, Ind. Eng. Chem. Fundam. 22 (1983) 105–109.
[34] Y. Ogawa, D. Huin, H. Gaye, N. Tokumitsu, Physical model of slag foaming, ISIJ Int. 33 (1) (1993) 224–232.